Rheology and Microstructure of an Unentangled Polymer Nanocomposite Melt

Benjamin J. Anderson and Charles F. Zukoski*

Department of Chemical and Biomolecular Engineering, University of Illinois at Urbana−Champaign, 600 South Mathews Ave, Urbana, Illinois 61801

Received June 24, 2008; Revised Manuscript Received October 17, 2008

ABSTRACT: The rheology and microstructure of 44 nm diameter silica particles suspended in unentangled polyethylene oxide (PEO) melts are studied through measurement of filled melt viscosity and X-ray scattering measurement of interparticle structure factors, $S(q,\phi_c)$, where q is the scattering vector and ϕ_c is the silica volume fraction. The neat polymer melts are Newtonian over the probed shear range. Filled melts have a constant viscosity at low particle concentrations and shear thin at high concentrations. At the same particle volume fraction, filled melt viscosities increase with polymer molecular weight. By defining an effective particle volume, assuming polymer adsorption adds $2.9R_g$ to the particle diameter, suspension viscosities of both molecular weights at all volume fractions resemble that of hard sphere suspensions. The particle osmotic compressibility and position and coherence of the first nearest neighbor shell suggest that the particles have radii larger than the core size due to polymer structuring near the particle surface. These results are interpreted as resulting from a modest strength of attraction between polymer segments and particle surfaces.

I. Introduction

Filled polymers are an important class of materials where particles are dispersed in a polymer matrix. When the particle reaches nanosized dimensions, the material is commonly referred to as a polymer nanocomposite. Particles are incorporated to improve and alter mechanical, electrical, optical, thermal, and/or barrier properties of the polymer.[1] The degree of property enhancement achieved in the composite depends on the state of the particle dispersion and the ability of the particle surface to alter polymer segment dynamics.[1,2] This makes dispersion of particles and control of the state of dispersion of considerable importance in the manufacture of nanocomposite materials.

The state of dispersion is sensitive to the forces that act between particles dispersed in polymer and how these forces drive particle organization. Over the past decade, there has been growing interest in understanding the fundamental chemistry and physics that govern the state of particle aggregation in a polymer melt and there is substantial evidence that the state of the dispersion depends on both particle−particle and polymer segment−particle surface interactions. A favorable segment−particle interaction leads to the polymer wetting the particle surface. The effects of attractions are, however, nonmonotonic, with weak attractions leading to particle stability and strong attractions leading to polymer bridging and aggregation.

In low molecular weight solvents, the interaction of solvent molecules with a surface results in structuring of the fluid next to the surface. As two surfaces are brought together, this structure results in solvation forces that can persist to surface separations of 5−10 molecular diameters. The force profile is oscillatory with a period equal to the molecular size and overlays a van der Waals attraction.[3] The amplitude of the oscillations increase near the surface. Solvation forces which arise from favorable interactions between the solvent and the surface tend to stabilize particles due to the work required to displace solvent molecules when particles are forced together. As the molecular weight of the solvent increases, theory and simulations suggest the characteristic length scale of the structuring remains the polymer segment diameter, as opposed to the polymer radius of gyration. Local structuring is predicted to protrude 2−3 segment diameters from a surface after which segmental density fluctuations are expected to be equivalent to the bulk.[4−6] The more rapid decay of the local structuring in linear polymer solvents is due to the configurational entropy penalty of a chain molecule assuming a more ordered configuration. The degree of polymer structuring at the particle surface is predicted to be sensitive to segment−surface interactions with stronger interactions resulting in greater structuring.

The results of the theory and simulations are not in agreement with experimental studies of the forces between surfaces when the interposing material is a polymer melt. The most detailed experimental studies are those that employ the surface forces apparatus (SFA),[7−14] but also more recently the atomic forces microscope (AFM).[15,16] These experiments measure the forces required to hold two surfaces at a particular separation and suggest the existence of an immobilized polymer layer on the two opposing surfaces with a thicknesses that depends on the polymer radius of gyration (R_g). As two surfaces are brought into close proximity, a monotonic repulsion appears initially at $5-6R_g$ and reaches a hard wall repulsion at $2-3R_g$.[7,10] Oscillatory interactions are rarely seen.[9] Evidence of a repulsion with ranges that scale on R_g has been seen for polydimethylsiloxane,[8,9,14−16] polyphenylmethylsiloxane,[7,10,14] polybutadiene,[11,12] and perfluorinated polyethers[13] on a number of surfaces such as mica and silica. Dynamic measurements of confined polymer below the entanglement molecular weight suggest that for surface separations greater than that associated with the adsorbed layer, the viscosity of the confined polymer is comparable to the bulk viscosity and there is a no-slip boundary condition located at $\sim 2R_g$ from the particle surface.[7,9,14] As surface separations become equivalent to the thickness of the adsorbed layer, polymer wall slip occurs at the plate surface.[59]

The general explanation for the discrepancy between predictive models and experiments is the slowing down of polymer dynamics at adsorbing surfaces. de Gennes suggested that if the segment interaction with the surface is sufficiently strong, the surface will "pin" polymer segments.[17] This would result in a monotonic repulsion that extends of order R_g from a surface. For a polymer molecule to change its configuration upon confinement between two surfaces, all adsorbed segments must desorb to allow the chain to change its configuration. The chain

* Corresponding author. E-mail: czukoski@illinois.edu.

10.1021/ma801415e CCC: $40.75
Published on Web 11/11/2008

nature of polymers enables many segments to adsorb per chain. If the strength of segment adsorption is strong, the polymer may be unable to adjust its configuration within a reasonable time scale. This hypothesis agrees with the later simulation study of Mansfield and Theodorou who show that strong adsorption leads to a flattened chain conformation and a lengthening of the relaxation time of chains whereas weak adsorption leads to higher segment mobility near a surface.[6] As a result, experimental studies of systems involving polymers and surfaces may not be capable of probing the equilibrium adsorption studied by models and simulations.

These phenomena are relevant to understanding the behavior of nancomposite melt flow properties. Similar questions about the strength and range of the particle interactions are important as are questions of the ability of the polymer to reach equilibrium configurations.[4−6,18] While few systematic studies have been undertaken, the few that have been performed report varying rheological responses that depend on the composition and size of the particle and the composition of the matrix. When the particle is of colloidal size (10 nm to 1 μm), the flow properties of the melt are enhanced resulting in an elevated nonlinear viscosity and enhanced elastic and viscous moduli.[19−23] However, when the particle reaches a size comparable to the polymer segment size, the viscosity is reported to decrease.[24] The magnitude of the change in mechanical properties and the state of the particle dispersion is also shown to depend on surface chemistry.[22,25,26]

Previously, we established that silica nanoparticles are stable in low molecular weight PEO melts through measurement of the particle second virial coefficients that were found to be positive, slightly larger than those expected for pure volume exclusion and to have a small dependence on polymer molecular weight.[27] One interpretation of these observations builds on the experimental work on measurements of surface forces suggesting that a buildup of an immobilized polymer layer on the surface produces a net repulsion between two particles. The surface forces experiments would suggest that the range of the repulsion will depend on R_g, thus contradicting the observation that the second virial coefficient is weakly dependent on R_g. The second explanation builds on the results of Hooper and Schweizer[28] who predict an oscillatory PMF with a period equal to the segment diameter. Under a range of conditions, the PMF is repulsive and integration over the PMF yields second virial coefficients greater than a hard particle volume exclusion value and a weak MW dependence.[28]

Here, we report our observations on the microstructure and flow properties of these silica particles in PEO melts outside the dilute limit. We find that at low volume fraction the melts are Newtonian over the measurable range of shear rates and the volume fraction dependence of the viscosity is consistent with surface force measurements indicating a thin layer of polymer is immobilized at the particle surface. The thickness of this layer scales on the polymer radius of gyration. If the immobilized layer thickness is held constant, the nanocomposite melts have low shear rate viscosities consistent with that of hard spheres up to effective volume fractions of 0.57. The structure factors characterizing particle packing are not consistent with this interpretation and show that the particles experience an effective repulsive force with a range significantly larger than that suggested by the viscosity measurements and that the magnitude of this repulsive force diminishes as the particle volume fraction increases. However, interpretation of the microstructural results is not as straightforward as that of the flow properties and provides some evidence that the systems are not at equilibrium. We have chosen to work with low molecular weight polymer melts to avoid the complication introduced by entanglements in the filled melt. Our system is similar to the nanocomposite system of Zhang and Archer, but the complications of long relaxation dynamics of high MW polymer and entanglement dynamics has been removed so that particle enhancement in polymer nanocomposites can be more clearly defined.[22] While one might expect particles suspended in these low MW polymers to behave as if they are suspended in a viscous, Newtonian phase, our results demonstrate that the connectivity of segments clearly affects the filled melt mechanical behavior and particle microstructure in ways that are not observed for particles suspended in low molecular weight solvents. In section II, we describe sample preparation methods and our experimental procedure. In section III, we present rheology and scattering results and discuss their implications as far as how particles influence the viscosity of the melt and how particles pack in the melt. In section IV, we offer concluding remarks.

Table 1. Polymer Properties

MW	N^a	R_g [nm]	T_m [°C]	$\eta_p{}^b$ [mPa s]
PEO400	9	0.8	8	16
PEO1000	23	1.3	40	35

[a] Number of monomers. [b] Temperature of 75 °C.

II. Experimental Methods

A. Sample Preparation. Silica particles were synthesized by the base catalyzed hydrolysis and condensation of tetraethylorthosilicate according to the method of Stöber et al.[29] The synthesis produces an alcosol solution of silica particles. Particles were synthesized with a number average diameter of 43 nm and a standard deviation of 4 nm as determined from TEM measurements. We predict a particle to segment size ratio of 35 based on a Kuhn segment diameter, d, of 1.2 nm ($d = C_\infty l/[\cos(\theta_p/2)]$, where $C_\infty = 6.9$ is the experimental characteristic ratio of PEO,[30] $l = 1.5$ Å is the length of a backbone bond, and $\theta_p = 68^o$ is the angle of a backbone bond). The Kuhn segment size is bigger than the PEO monomer size which is 0.4 nm. A number average particle diameter, D_c, of 43 nm was chosen as a compromise between minimizing D_c/d and our ability to synthesize well defined monodisperse particles. Particles were dispersed in unentangled PEO of two MW purchased from Sigma-Aldrich (the molecular weight of entanglements of PEO, $M_{e,PEO} \approx 2000$). Properties of the polymers are listed in Table 1. The R_g values were calculated from the characteristic ratio of PEO in the melt.

After particle synthesis, the alcosol was concentrated 10 times by heating in a ventilation hood. This concentration step drives off water and ammonia from the alcosol. Particle dispersions were made by combining known masses of the alcosol and PEO. The ethanol was evaporated at a temperature above the melting point of PEO under vacuum. PEO is miscible in ethanol above a temperature that is just below its MW dependent melting temperature ($T_{m,PEO400} = 8$ °C, $T_{m,PEO1000} = 40$ °C).[31] Samples are heated in a vacuum oven to drive off ethanol. The vacuum oven was purged several times with nitrogen followed by evacuation of the chamber to remove oxygen which degrades PEO at high temperature. Once the ethanol is visibly gone, samples were further heated to 75^oC in a vacuum oven for 48 h to drive off any residual ethanol. There were no changes in the mechanical properties when heating for an additional 48 h. When heating the samples for long times, several weeks, the viscosity of the samples would slowly decline. This drop in the viscosity was also seen for the neat polymer and is attributed to polymer degradation when heated for long times. Rapid degradation was seen to occur if the chamber is not effectively evacuated. Excessive temperatures were avoided due to the possibility of grafting PEO to a silica surface.[32,33]

The amount of alcosol added to a known mass of PEO was determined by the desired amount of loading once the ethanol was evaporated. The alcosol is combined with the PEO at a temperature above T_m of the polymer followed by a rapid mix on a vortex stirrer. The resulting mixture is a light near transparent blue reminiscent

of the alcosol before the addition of PEO. Once the ethanol is evaporated, the filled polymer is transparent since PEO and silica are contrast matched. This index matching reduces the Van Der Waals forces between the particles.[34] When suspensions are index matched in low MW solvents and the characteristic size of the solid phase is much bigger than the dispersing phase, the dispersing phase can be viewed as a continuum. Under such conditions, suspension microstructure and rheology is seen to be well described by hard sphere models.[35] The particle mass fraction of the alcosol was measured by dry weight after evaporation of the ethanol. The density of the particle filled melt, ρ_T, was measured using a Mettler/KEM DA-100 density/specific gravity meter. The particle volume fraction, ϕ_c, was calculated from the mass of silica, m_c, added to a mass of polymer, m_p, using the measured filled melt density and a particle density, ρ_c, of 1.6 g/cm^3 determined from the particle molecular weight and particle size.[27]

$$\phi_c = \frac{\rho_T}{\rho_c}\left(\frac{m_c}{m_c + m_p}\right) \tag{1}$$

B. Rheology. Rheological experiments were performed using a constant stress C-VOR Bohlin rheometer with cone and plate geometry. The cone diameter was 20 mm, and the angle was 4°. Measurements were made at a sample temperature of 75 °C. This temperature was chosen because it is above the melting temperature of PEO for all molecular weights. The melting temperature of high MW PEO is 66 °C. Viscosity measurements were made on samples prepared in two different ways. Samples were first made by evaporation of alcohol to produce a filled melt with the desired particle volume fraction. The second set of samples were made by first preparing a highly concentrated filled melt ($\phi_c = 0.46$ for PEO400 and $\phi_c = 0.43$ for PEO1000) followed by dilution with additional polymer to the desired volume fraction. The purpose of this procedure is to ensure that the synthesis condition is not affecting the adsorbed conformation of the polymer on the particle surface. Viscosity measurements of both sample sets were identical.

C. SBUSAXS. SBUSAXS was performed at the 32ID-B XOR beam line located at the Advance Photon Source, Argonne National Laboratory. The instrument employs a Bonse-Hart camera and a double-crystal Si(111) optics to extend the range of measurements to lower scattering vectors.[36] A pair of horizontally reflecting crystals enabled effective pinhole collimation removing the need for slit desmearing. An absolute calibration converts scattering intensity from counts per second to absolute units of cm^{-1} through knowledge of the sample thickness along the path of the beam. Samples were loaded in custom-made aluminum cells. Two kapton polyimide slides sealed the sides of the cell chamber using epoxy perpendicular to the beam path. The beam path length was approximately 1 mm. The cells were heated to 75 °C and maintained by a constant temperature water bath. Measurements on each sample were taken over a period of 30 min. Background intensity was accounted for by measuring the scattered intensity of neat PEO. The scattering intensity of the PEO is subtracted off of the sample scattering leaving only scattering due to the silica nanoparticles. This is based on the fact that the scattering from the silica particles dominates leading to our assumption that cross scattering terms between the polymer and particle can be neglected and the dispersion can be viewed as an effective one component system.[37−40]

The scattering intensity of X-rays from a single component dispersion is given by

$$I(q,\phi_c) = \phi_c V_c \Delta\rho_e^2 P(q) S(q,\phi_c) + B \tag{2}$$

The first term refers to scattering from the particles where ϕ_c is the particle volume fraction, V_c is the volume of a single particle, and $\Delta\rho_e$ is the electron scattering length density of the particles over that of the PEO dispersing phase. The variable q is the scattering vector, $q = (4\pi/\lambda)[\sin(\theta/2)]$, where λ is the wavelength of incident X-rays and θ is the scattering angle. $P(q)$ is the form factor accounting for intraparticle scattering interference and $S(q,\phi_c)$ is the structure factor accounting for interparticle scattering interference. The second term, B, refers to background scattering and scattering from the polymer. Background scattering and polymer scattering is subtracted off of the intensity by the scattering of a reference which in our case is the neat polymer. From this point on, $I(q,\phi_c)$ will refer only to scattering from the particles.

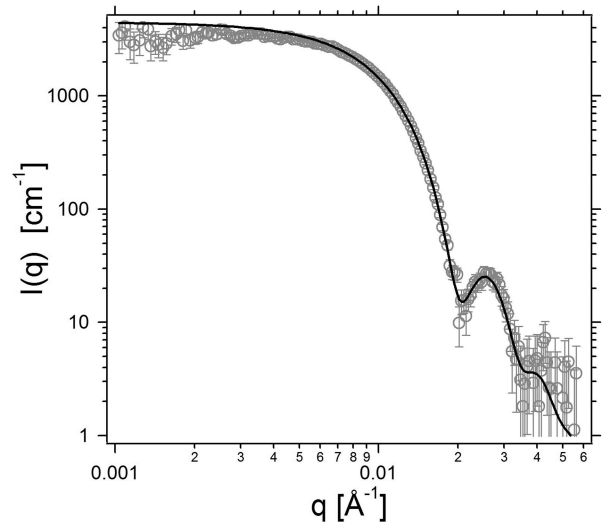

Figure 1. Experimental scattered intensity and model fit [solid line] of a dilute suspension ($\phi_c = 0.022$) of particles in PEO1000 utilizing an average form factor, $\bar{P}(q)$. Fitting parameters are $\bar{D}_c = 44$ nm, $\nu = 4$ nm, $\Delta\rho_e = 6.5 \times 10^{10}$ cm^{-2}.

In the dilute particle limit, the structure factor goes to unity and the scattering equation reduces to $I(q,\phi_c) = \phi_c V_c \Delta\rho_e^2 P(q)$. The form factor for spherical particles is given by

$$P(q) = \left(3\frac{\sin(qD_c/2) - (qD_c/2)\cos(qD_c/2)}{(qD_c/2)^3}\right)^2 \tag{3}$$

We account for modest polydispersity in particle size by calculating $P(q)$ for a size distribution. This is done by employing a Gaussian diameter distribution to calculate an average form factor for a population of particles with volume average diameter $\bar{D}_c$ and standard deviation ν. The integration variable D_c is the variable diameter of a particle.

$$\bar{P}(q) = \frac{\int \frac{1}{\sqrt{2\pi\nu^2}} e^{(-(D_c - \bar{D}_c)^2/2\nu^2)} D_c{}^6 P(q)\, \mathrm{d}D_c}{\int \frac{1}{\sqrt{2\pi\nu^2}} e^{(-(D_c - \bar{D}_c)^2/2\nu^2)} D_c{}^6\, \mathrm{d}D_c} \tag{4}$$

Experimental scattering of dilute suspensions are fit to the scattering equation for $q > 0.007$ Å^{-1} utilizing eq 4 for the form factor to determine a scattering size and standard deviation in the polymer melt (Figure 1). The depression in the scattering at low q in Figure 1 is due to the influence of $S(q,\phi_c)$ which is not truly unity at all q, but less than unity at low q. The fitting procedure has three adjustable parameters: particle diameter, standard deviation, and electron contrast density.

As the volume fraction of particles is raised, the structure factor measures the spatial distribution of particles in inverse space. Formally, the structure factor for a single component dispersion is defined as the Fourier transform of the nonrandom part of the pair correlation function, $g_{cc}(r)$.

$$S(q,\phi_c) = 1 + \frac{\phi_c}{V_c}\int_0^\infty 4\pi r^2 [1 - g_{cc}(r)]\frac{\sin(qr)}{(qr)}\, \mathrm{d}r \tag{5}$$

The term $[1-g_{cc}(r)]$ is often called the total correlation function, $h_{cc}(r)$. In order to determine the real space distribution of particles, one must take the inverse Fourier transform of $S(q,\phi_c)$ to find $g_{cc}(r)$.

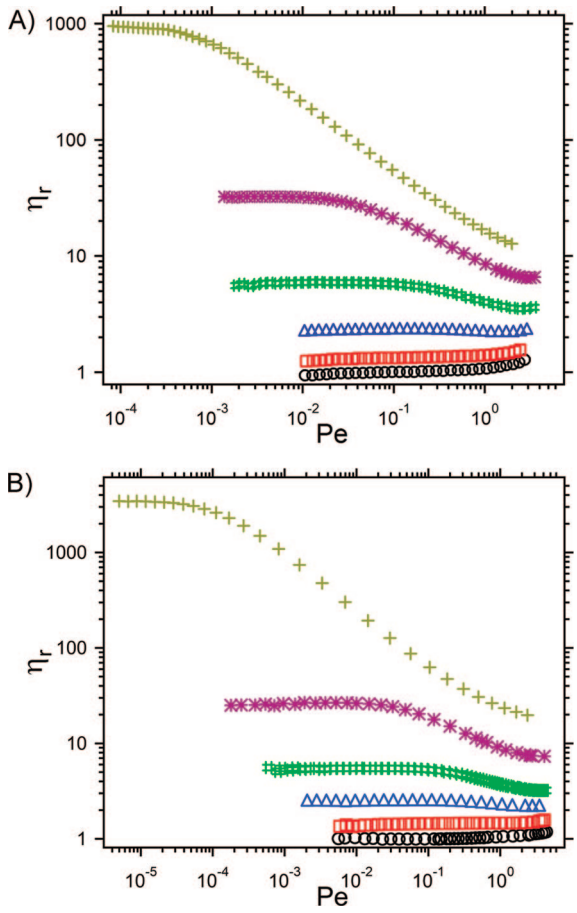

Figure 2. Measurement of the relative viscosity versus *Pe* of (A) PEO400 for ϕ_c of 0.000 [○], 0.095 [□], 0.193 [△], 0.296 [#]0.410 [∗], 0.480 [+] and (B) PEO1000 for ϕ_c of 0.000 [○], 0.091 [□], 0.177 [△], 0.270 [#], 0.373 [∗], 0.445 [+].

Experimental structure factors for concentrated suspensions are calculated by dividing the intensity of a concentrated suspension by the intensity of a dilute suspension (ds), eq 6. In the dilute limit, the structure factor goes to unity since particle positions are uncorrelated. The result leaves $S(q,\phi_c)$ for the concentrated suspension,

$$S(q,\phi_c) = \frac{I(q,\phi_c)}{I_{ds}(q,\phi_c)} \frac{\phi_{c,ds}}{\phi_c} \tag{6}$$

III. Results and Discussion

A. Rheology. In Figure 2, the steady state relative viscosity, $\eta_r = \eta/\eta_p$, is plotted as a function of the dimensionless Peclet number ($Pe = 6\pi\eta_p\dot{\gamma}R_c^3/k_BT$, η_p is the viscosity of the polymer, R_c is the particle radius, $\dot{\gamma}$ is the shear rate, k_B is Boltzmann's constant, and T is temperature). The neat low molecular weight polymers behave as Newtonian liquids with viscosities of 16 cP and 35 cP at 75 °C, respectively. At low particle concentration ($\phi_c \leq 0.1$), the melt viscosities are also independent of shear rate. The slightly elevated viscosity at high *Pe* is due to secondary flows not associated with the particles. A small amount of shear thinning is present at ϕ_c of 0.193 and 0.177 in PEO400 and PEO1000 respectively. Shear thinning in stable particle suspensions is a many body effect and appears as three-body and higher order interactions become significant.[41] These interactions create thermodynamic stresses. At low shear rates thermodynamic stresses dominate over hydrodynamic stresses and elevate the low shear viscosity. At higher particle volume fractions, shear thinning is observed. Shear thinning occurs as hydrodynamic stresses alter the suspension microstructure. At high *Pe*, the viscosity reaches a second plateau. The behavior observed for the flow properties of the silica particles in these low MW polymers (high MW solvents) is similar to the behavior of stable particle suspensions in low MW solvents: viscosities dominated by Brownian type interactions at low rates of deformation and viscosities dominated by hydrodynamic interactions at high rates of deformation.[41]

Due to the Newtonian behavior of unentangled PEO melts and the large polymer-particle size ratio, we make the assumption that the low MW polymer-particle composite may be viewed as a particle suspension in a high viscosity continuum.

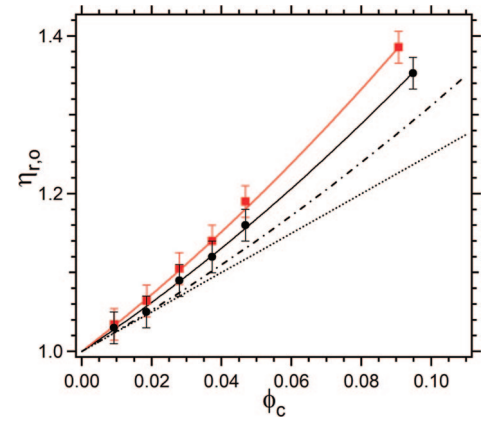

Figure 3. Measurement of the zero shear rate viscosity of PEO400 [●] and PEO1000 [■] are plotted versus ϕ_c. Also shown are Einstein's equation [dotted line], Einstein's equation including the hard sphere second order correction [dot-dash line], and fits to eq 7 [solid lines].

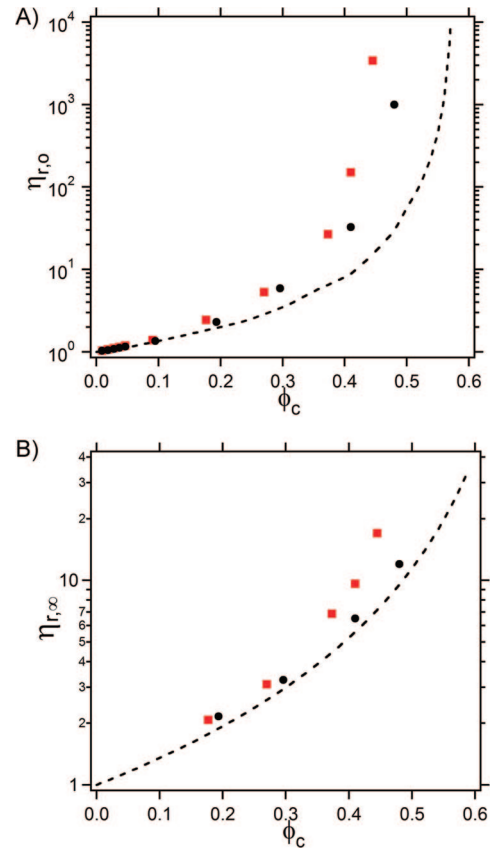

Figure 4. Measurement of (A) the low shear rate viscosity and (B) the high shear rate viscosity for PEO400 [●] and PEO1000 [■] nanocomposites are plotted versus ϕ_c [closed symbols]. Also shown is a smooth curve through experimental hard sphere data [dashed line] plotted as a function of volume fraction.[43,44]

Table 2. Relative Viscosity Fitting Parameters

PEO400				PEO1000			
ϕ_c	ϕ_η	σ_c	m	ϕ_c	ϕ_η	σ_c	m
0.193	0.227	0.087	3.2	0.177	0.227	0.089	1.92
0.296	0.348	0.13	1.79	0.270	0.348	0.11	1.73
0.410	0.482	0.13	1.63	0.373	0.479	0.13	1.62
0.480	0.564	0.051	1.70	0.410	0.527	0.082	1.45
				0.445	0.572	0.030	1.75

Under this premise, the low shear relative viscosity, $\eta_{r,o} = \lim_{Pe\to 0}\eta_r$, of stabilized particles at low volume fractions in a solvent may be characterized by

$$\eta_{r,o} = 1 + 2.5k\phi_c + H(k\phi_c)^2 \quad (7)$$

where $k = \phi_{eff}/\phi_c$, ϕ_{eff} is an effective volume fraction, and H accounts for particle pair interactions. We expect $H = 5.9$ if the particles interact as hard spheres.[42] In Figure 3, $\eta_{r,o}$ is fit to eq 7 by a least-squares nonlinear regression for $\phi_c \leq 0.10$ yielding $k = 1.18 \pm 0.04$ and 1.34 ± 0.05 and $H = 6 \pm 1$ and 6 ± 1 for PEO 400 and 1000 respectively. The values of k imply that the particles look effectively larger and the values of H compare well to the theoretical value of 5.9 expected of hard sphere suspensions. These dilute solution results suggest that particles behave as hard spheres with sizes that are larger than the core silica particle. In Figure 3, closed symbols are $\eta_{r,o}$ measurements at low volume fractions plotted versus ϕ_c. Also shown are the predictions of Einstein's equation ($\eta_{r,o} = 1 + 2.5\phi_c$), Einstein's equation with the second order correction for hard spheres ($\eta_{r,o} = 1 + 2.5\phi_c + 5.9\phi_c^2$), and the fitting results to eq 7. The observation that k is greater than unity and H is equivalent to the hard sphere value suggests that particles have a larger effective hydrodynamic size and that interactions can be characterized by a hard repulsion.

In Figure 4, $\eta_{r,o}$ is plotted as a function of ϕ_c as closed symbols over the full volume fraction range studied. When comparing $\eta_{r,o}$ to the viscosity measured of experimental hard sphere suspensions,[43,44] the particles again appear to occupy a volume larger than their core size. (Figure 4A). Secondary flows at high shear and loss of sample from spinning out of the cone and plate gap in some cases hindered absolute measurement of the high shear relative viscosity, $\eta_{r,\infty}$. The values shown in Figure 4B are from fitting η_r with eq 8 to extrapolate to the high shear plateau.

$$\eta_r = \eta_{r,\infty} + \frac{\eta_{r,o} - \eta_{r,\infty}}{1 + (\sigma_r/\sigma_c)^m}, \quad \sigma_r = \frac{\sigma R_c^3}{k_B T} \quad (8)$$

σ_r is the reduced shear stress, σ_c is a dimensionless critical stress, and m is a fitting parameter. Values of σ_c and m are shown in Table 2. σ_c are similar to those observed for hard sphere-like particles suspended in low molecular weight continuous phases, and also indicates a maximum critical stress.[45] $\eta_{r,\infty}$ is found to also be elevated above the high shear viscosity measured of experimental hard spheres (Figure 4B).[44] The elevation is higher as the MW is increased.

In Figure 5, $\eta_{r,o}$ and $\eta_{r,\infty}$ are plotted versus ϕ_η where $\phi_\eta = k_\eta\phi_c$. k_η is an adjustable parameter that accounts for the larger effective size of the particles due to polymer adsorption. We find that these data at all volume fractions for the two melts collapse onto a single curve at low Pe that superimpose on the experimental data of hard sphere-like suspensions.[43,44] The data also collapse at high Pe, but the viscosity as a function of ϕ_η drops convincingly below hard spheres at $\phi_\eta > 0.3$.[44] The values of k_η that collapse the data are found to depend similarly on polymer molecular weight following the relation $k_\eta = (D_\eta/D_c)^3 = [1+(2.9R_g/D_c)]^3$. The values of k_η are 1.18 ± 0.01 and 1.29 ± 0.02 for PEO 400 and 1000 respectively which agree quiet well with k determined from the fitting of the dilute viscosity data to eq 7. The quantity D_η/D_c, where D_η is an effective particle diameter, is 1.06 and 1.09 for PEO 400 and 1000, respectively. The dependence of k_η on R_g indicates that effective hard sphere size depends on polymer molecular weight suggesting that the range of the effective hard sphere repulsion is governed by the degree of polymerization, not by polymer segment size.

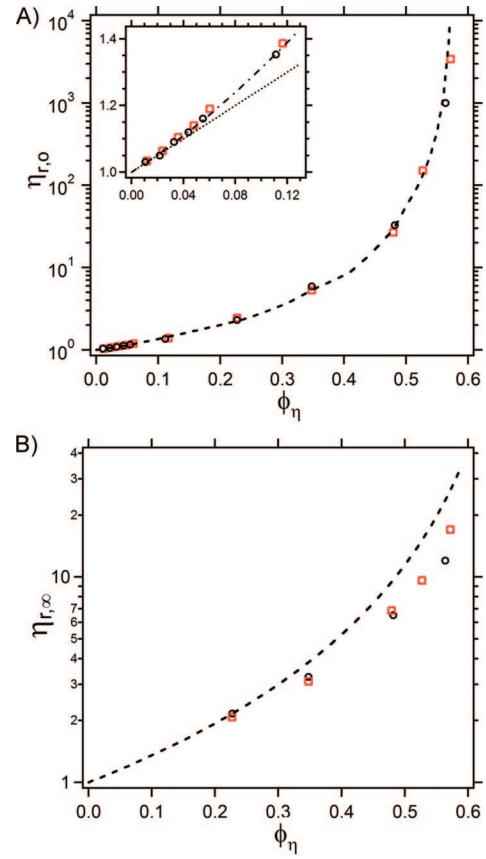

Figure 5. Measurement of the (A) zero shear rate viscosity and (B) the high shear rate viscosity for PEO400[○] and PEO1000 [□] nanocomposites are plotted versus ϕ_η [open symbols]. The inset (A) shows the low shear viscosity at low volume fractions. Also shown are Einstein's equation [dotted line], Einstein's equation with the hard sphere second order correction [dot-dash line], and a smooth curve through experimental hard sphere data [dashed line] plotted as a function of volume fraction.[43,44]

When comparing the low shear viscosity to that observed for hard spheres, the polymer layer has a constant thickness up to ϕ_η of 0.57. The average particle surface to surface separation in terms of R_g at this volume fraction can be estimated from $a_{cc} = (D_c/R_g)[(\phi_m/\phi_c)^{1/3} - 1]$ where ϕ_m is the maximum random packing fraction of 0.63. When $\phi_c = 0.445$ ($\phi_\eta = 0.572$) for PEO1000, $a_{cc} = 4.1$ indicating that at this volume fraction the adsorbed layers are not yet overlapping. Thus, filled melt viscosity is well described by effective hard spheres suspended in a Newtonian continuous phase even when the distance available for polymer between the effective hard core particle surface is of order $2R_g$. These results indicate that the particles interact like hard spheres with a size that depends on polymer molecular weight, but not volume fraction, suspended in a continuous phase with a molecular weight dependent Newtonian viscosity.

The high shear viscosity drops below hard spheres at high particle volume fractions. Our initial intuition is that this is a result of the softness of the adsorbed polymer layer. The high shear viscosity clearly deviates from hard spheres at $\phi_\eta > 0.3$.

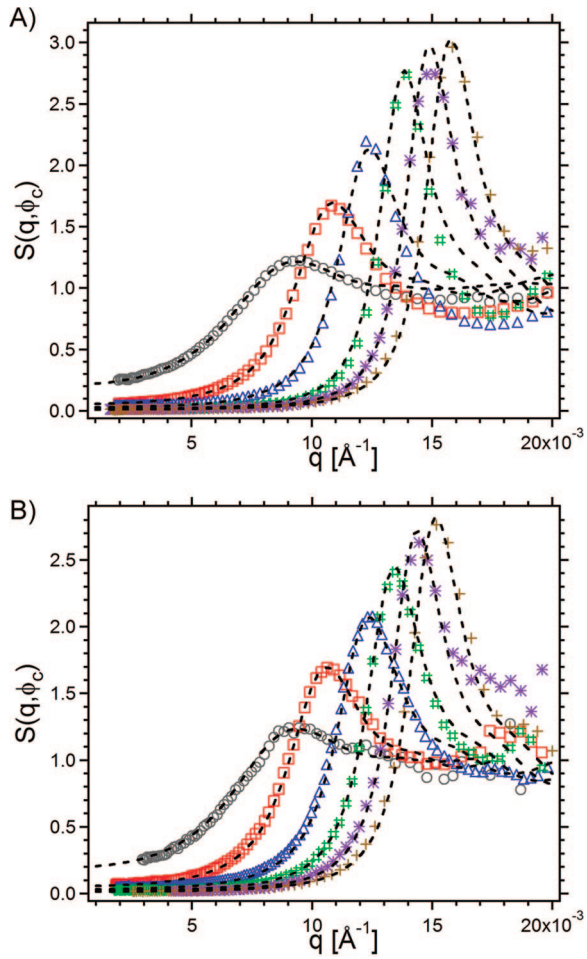

Figure 6. Particle structure factors of (A) PEO400 at a ϕ_c of 0.095 [○], 0.193 [□], 0.296 [△], 0.410 [#] 0.514 [∗], 0.550 [+] and (B) PEO1000 at a ϕ_c of 0.091 [○], 0.177 [□], 0.270 [△], 0.373 [#], 0.473 [∗], 0.520 [+]. Dashed lines are model fits to polydisperse hard sphere structure factors using two adjustable parameters: the effective particle volume fraction, $\phi_{S(q)}$, and the effective particle diameter, D_{q^*}.

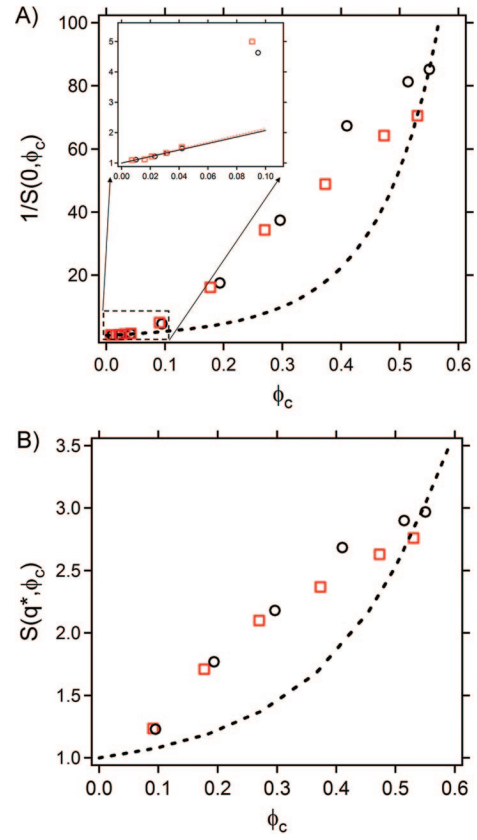

Figure 7. (A) Particle inverse compressibility ($1/S(0,\phi_c)$) and (B) the magnitude of the first structural peak ($S(q^*,\phi_c)$) plotted versus ϕ_c for PEO400 [○] and PEO1000 [□]. Also shown is the expected curves of a hard sphere suspension [dashed lines].

It is difficult to know if the high shear viscosity deviates at lower volume fractions since secondary flows hinder measurement at higher shear. Interestingly, the high shear viscosity of suspensions of soft particles fall off the effective hard sphere curve as the volume fraction exceed 0.3 suggesting that deviation of the high shear viscosity may be associated with soft particle interactions.[46] These same suspensions also show deviation of the low shear viscosity from hard sphere behavior as well.

Recently, working at shear rates that are extreme compared to those probed experimentally here, Pryamitsyn and Ganesan silmulated the flow of nanoparticles in an unentangled polymer melt and showed that polymer slip increased with polymer molecular weight when there are weak attractions between polymer segments and the particles. These simulations were carried out with particles having a diameter of five segment diameters and did not show an increased effective particle size with polymer molecular weight.

Wyart and de Gennes hypothesized that polymer slip at a particle surface can lower the friction factor associated with particles in a polymer matrix.[47] This effect diminishes as the particle size becomes larger than the Edward's tube diameter,[48] However in the large particle limit, with increasing strength of segment−particle attraction, they suggest that the effective particle hydrodynamic size will increase by $\sim R_g$ due to nonslip of polymer segments at the surface.

While models and simulations consistently show the length scale for polymer melt modulated surface interactions is the segment diameter, confined melt experiments consistently show monotonic repulsive profiles that scale on the polymer radius of gyration.[7−16] For example, Granick and co-workers report the force profile of PPMS on mica for several molecular weights all below M_e.[7] In their work, the polymers used are similar in size (R_g) and number of skeletal bonds to that of PEO 400 and 1000. They observe a monotonic repulsion that increases in an exponential fashion and report that the required force to hold surfaces at a fixed separation for different molecular weights collapse onto a single curve when the plate separation is normalized by R_g. The repulsive force becomes appreciable ($\sim 1\ k_BT$) at a spacing of $\sim 4.5\ R_g$ and is strongly repulsive approaching a hard wall interaction when the surfaces have a separation of $2.8\ R_g$. When measuring the dynamic response, the confined polymer displayed a viscosity comparable to the bulk viscosity at surface separations of $7R_g$, but transitioned to an elastic response at separation distances of $<5R_g$.

In the present study, the minimum average particle separation probed is $4.1R_g$ for PEO1000 at $\phi_c = 0.445$. At this volume fraction, the filled melt has a well defined low shear viscosity suggesting that free polymer is present between the particles with a viscosity comparable to the bulk viscosity. The adsorbed PEO appears to form a more compact layer than PPMS.

Schools of thought on the origin of the R_g scaling of the repulsion include that of de Gennes where polymers assume an extended configuration.[17] The repulsion is described by the pinning of segments to the surface such that the polymer molecules cannot adjust their configurations on a reasonable time scale as they become confined thus trapping them in a "restricted" equilibrium configuration. Mansfield and Theodorou appear to explain the pinning effect as arising from high potential barriers at segment adsorption sites which impedes

lateral motion of chains and lengthens the relaxation time.[6] A second explanation invokes nonequilibrium adsorption where the first polymers to adsorb assume a flat configuration while polymers that adsorb later assume an extended configuration due to lower availability of adsorption sites.[49] In this case, the strength of segment-surface interactions hinders equilibration of the adsorbed segments. These two explanations highlight an ongoing debate over equilibrium versus nonequilibrium polymer adsorption. Both approaches argue that repulsive interactions have ranges that will scale on R_g. Our mechanical studies cannot distinguish between the two, but do confirm the existence of a monotonic repulsion that scales with R_g and appears to stabilize particles.

B. SBUSAXS. Based on the collapse of the low shear viscosity data onto data predicted and measured for other hard sphere-like suspensions, we would expect the static microstructure of the particles in PEO to mimic effective hard particles of a slightly larger size. Figure 6 shows the particle structure factors of moderately low to high particle concentration in PEO400 and PEO1000. The particles display liquid like character in both molecular weights up to volume fractions greater than 0.50.

Given our interest in the effective particle volume fraction developed from the comparison of the filled polymer viscosities with values predicted for hard spheres, we initiate our investigation of the particle microstructure by the ability of hard spheres to capture the inverse particle compressibility, $\partial\Pi/\partial\phi_c$, which is measured through Eq. (9) by extrapolating to $S(0,\phi_c)$.

$$\lim_{q\to 0}\frac{1}{S(q,\phi_c)}=\frac{V_c}{k_BT}\frac{\partial\Pi}{\partial\phi_c} \tag{9}$$

Π is the osmotic pressure. The results shown in Figure 7A include data presented in Figure 6 and several addition dilute measurements. The two lines in the inset of Figure 7A are a linear fit of the dilute measurements to a first order virial expansion in Eq (10).

$$\lim_{q\to 0}\frac{1}{S(q,\phi_c)}=\frac{V_c}{k_BT}\frac{\partial\Pi}{\partial\phi_c}=1+8\bar{B}_2\phi_c(\text{dilute}) \tag{10}$$

$\bar{B}_2$ is the particle second virial coefficient normalized by the particle excluded volume and is interpreted as a conversion factor between the colloid volume fraction and the effective hard sphere volume fraction, $\phi_{S(q)}/\phi_c$. As a result, we expect values of k_η and $\bar{B}_2$ to be similar and indeed we find that $\bar{B}_2 = 1.3 \pm 0.2$ and 1.4 ± 0.3 for PEO 400 and 1000, respectively. Thus, under dilute conditions, the suspension thermodynamic and hydrodynamic properties are well described as effective hard particles with sizes slightly larger than the core silica particle size.

For $\phi_c > 0.09$, there is a rapid rise in $1/S(0,\phi_c)$ suggesting a dramatic suppression of particle density fluctuations. $1/S(0,\phi_c)$ continues to grow rapidly upon further addition of particles. When compared to a hard sphere suspension in a low MW solvent at the same particle concentration (Figure 7A, dashed line), the particles in melts of both molecular weights are much less compressible than if the particles interacted only through volume exclusion interactions. At higher ϕ_c, the growth in the osmotic pressure slows and eventually approaches the hard sphere value.

The magnitude of $S(q^*,\phi_c)$ provides information about the coherence in the first nearest neighbor shell of particles. In Figure 7B, we compare the behavior of $S(q^*,\phi_c)$ measured in our melts with the behavior expected for hard spheres and observe behavior similar to the volume fraction dependence of $1/S(0,\phi_c)$. The dispersion is less compressible as the shell of nearest neighbor particles becomes more coherent due to suppressed particle density fluctuations. However, above a volume fraction of 0.3, the growth in $S(q^*,\phi_c)$ slows, and values of $S(q^*,\phi_c)$ approach those expected for hard spheres at a volume fraction of ϕ_c.

These data suggest that density fluctuations are suppressed over those expected for hard spheres and are more strongly correlated than expected for hard spheres of the same size as the core silica particles. However the decrease in compressibility and increase in coherence of the first shell of particles slows at higher volume fractions suggesting a softening of the repulsive interactions such that at the highest volume fractions the behavior approaches that of hard spheres with the core silica size. Note that the PEO1000 suspensions start with an effective size larger than the particles suspended in PEO400. However at higher volume fractions there are fewer density fluctuations and more coherence in the PEO400 composites.

Further analysis of the scattering data is found by forcing a fit of $S(q,\phi_c)$ by an effective hard sphere structure factor. Hard sphere structure factors are calculated using the Percus−Yevick closure through the method of Vrij and Baxter's simplification of the direct correlation function.[50−52] The model calculates the total scattering intensity of a suspension as a function of dimensionless scattering vector, qD, for an input volume fraction. A Gaussian particle size distribution is incorporated into the model to predict the scattering intensity of a polydisperse particle suspension. The particles are 10% polydisperse. Polydisperse structure factors are derived by dividing the total scattering intensity by the particle form factor.[51] The predictions of the model have been shown to predict the scattering intensity of polydisperse monomodal and bimodal particle populations.[53] Figure 6 shows the fits to the model.

The structure factors are fit to the model using two adjustable parameters: $\phi_{S(q)}$, an effective particle volume fraction and D_{q^*}, an effective particle diameter that captures the average spacing between the particles. The fitting procedure is as follows. First, $\phi_{S(q)}$ is selected that captures the magnitudes of $S(0,\phi_c)$ and $S(q^*,\phi_c)$. The model calculates the structure factor in dimensionless scattering vector space. Second, an effective hard sphere diameter, D_{q^*}, is selected such that the model fits the experimental structure factor in dimensional scattering vector space.

By allowing D_{q^*} to be independent of $\phi_{S(q)}$, the model captures in a near quantitative manner, the experimental structure factors. Notice that D_{q^*} only shifts the data in q space, but does nothing to the shape of the model structure factor. Below we discuss the implications of allowing D_{q^*} to be independent of $\phi_{S(q)}$. By forcing $S(0,\phi_c)$ to hard sphere values we extract an effective thermodynamic volume fraction, $\phi_{S(q)}$. Of significance is that the same value of $\phi_{S(q)}$ also predicts the magnitude of $S(q^*,\phi_c)$ and the shape of the first peak in $S(q,\phi_c)$ near q^* when the effective particle size is set to D_{q^*}. This demonstrates that the structure can be interpreted in terms of effective hard sphere behavior.

There are two important features of $\phi_{S(q)}$. First, for small values of ϕ_c, the effective particle volume fraction is slightly larger than the core particle size. With increasing ϕ_c, $\phi_{S(q)}$ passes through a maximum before returning to values near ϕ_c with increasing number density. (Figure 8). Second, the effective volume fraction is weakly dependent on polymer molecular weight. These features indicate that the thermodynamic and hydrodynamic particle sizes have different dependencies on silica volume fraction and polymer molecular weight.

In order to make a comparison between the effective particle sizes we define one final effective size from the PY fits to $S(q,\phi_c)$, $D_{S(q)} = D_c(\phi_{S(q)}/\phi_c)^{1/3}$. In Figure 9, we compare three measures of particle size as a function of ϕ_c. The hydordynamic sizes are dependent on molecular weight but have no dependence on ϕ_c. The thermodynamic sizes are not equal but are substantially larger than D_c at $\phi_c \sim 0.09$ and decrease toward D_c as ϕ_c

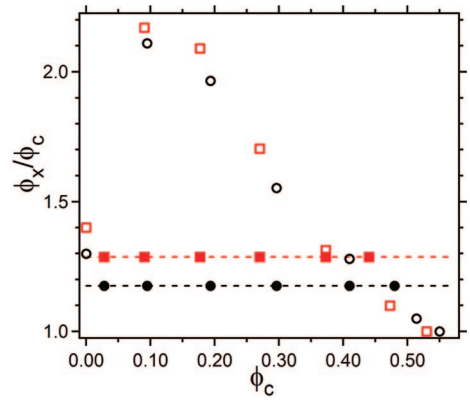

Figure 8. The normalized effective particle volume fraction based on the fit to hard sphere structure factors ($\phi_{S(q)}/\phi_c$) for PEO400 [○] and PEO1000 [□] and on the low shear rate viscosity (ϕ_η/ϕ_c) for PEO400 [●] and PEO1000 [■] versus ϕ_c.

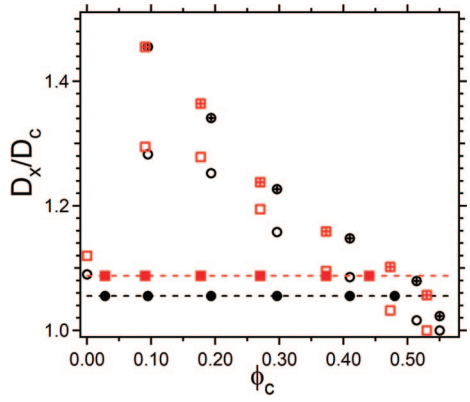

Figure 9. The normalized effective particle diameters plotted versus ϕ_c: D_{q^*}/D_c for PEO400 [⊕] and PEO1000 [⊞], $D_{S(q)}/D_c$ for PEO400 [○] and PEO1000 [□], and D_η/D_c for PEO400 [●] and PEO1000 [■].

increases. The maximum in the thermodynamic size suggests particles experience a long-range repulsion that is not important in determining the suspension viscosity.

The inability of effective hard spheres to describe the structure with a particle size and volume fraction that have similar dependencies on particle number densities suggests the hard sphere pair potential cannot describe particle packing behavior. In addition, the possibility of nonequilibrium polymer configurations may influence the packing and rheology in ways that are not captured in equilibrium descriptions of particle packing.

IV. Conclusion

Silica nanoparticles dispersed in unentangled PEO melts were studied using measurement of steady state filled melt viscosity and the particle static structure factor. Silica and PEO have near identical refractive indices such that VDW forces between the particles are minimized. Thus, particle stability is expected to be solely governed by polymer-surface interactions. Contrast matched particle suspensions in low molecular weight solvents where the solvent wets the surface are routinely well described by hard sphere models.[43,44] Here we explore the ability of particles dispersed in polymer melts to obey such models. Past experiments performed with high molecular weight filled entangled polymers show deviations, yet there is no consensus on the origin of the deviations: particle aggregation,[54] polymer bridging,[22] or a slowing down of polymer entanglements.[7,21,55] The present study focused on unentangled polymers where the complications of entanglements and long relaxation times in the bulk polymer are eliminated. In an attempt to demonstrate the equilibrium nature of the observations, we demonstrate that particle packing and flow properties are independent of the preparation path. The formation of the adsorbed layer is considered to be a "restricted" equilibrium or nonequilibrium phenomenon,[17,49] yet the adsorbed polymer consistently evolved to the same final state. We see no evidence of a change in the state of the dispersion or in rheological properties as the nanocomposite melt is sheared or annealed as was previously seen in high MW PEO−silica nanocomposites.[22] The viscosity of the unentangled PEO−silica nanocomposites diverges at high volume fraction suggesting the onset of a solid like response. Further studies are needed to discern the origin of elevated mechanical properties in PEO−silica nanocomposites below entanglement and as the MW of the polymer is increased.

The viscosity showed a well defined low shear viscosity, and shear thinning expected for colloidal suspensions in low molecular weight solvents. We conclude that the collapse of $\eta_{r,o}$ onto experimental hard spheres by increasing the size of the particles proves that the particles are interacting as effective hard particles with a larger size of $D_c + 2.9R_g$ in the polymer melt. The fact that the effective size of the particles scales with polymer R_g suggests that the effective hard particle interaction originates from adsorbed polymer on the particle surface. Scaling of adsorbed layers with R_g in contact with its melt has been seen previously in confinement studies of polymer melts.[7−16]

The similarity of the low shear viscosity as a function of ϕ_η to a hard sphere suspension suggests that the flow behavior is best understood through the flow mechanics of colloidal suspensions. At low particle concentrations, the viscosity is enhanced by particles with a larger effective hydrodynamic size due to polymer adsorption. The low shear viscosity is well described by colloidal models with a no-slip boundary condition located at a surface of shear $1.4R_g$ from the particle surface. At moderate particle concentrations where the dispersion is no longer considered dilute, three-body and higher-order interactions induce local structure in the density distribution of particles. The viscosity is enhanced by thermodynamic stresses at low *Pe* and hydrodynamic stresses at high *Pe*. The volume fraction dependence of the high shear viscosity is lower than the viscosity of hard spheres, yet still collapses onto a single curve for the two molecular weights studied with an effective particle size of $D_c + 2.9R_g$.

While rheology supports a hydrodynamic size that depends on an adsorbed polymer layer in direct contact with the particle surface, static scattering supports a different effective particle size based on the particle structure factor. The structure factors appear liquid-like and are well fit by a hard sphere model that employs the Percus−Yevick closure with an effective volume fraction, $\phi_{S(q)}$, and an effective particle diameter, D_{q^*}. The particle compressibility, however, does not mimic hard sphere behavior as a function of particle volume fraction. Instead $\phi_{S(q)}/\phi_c$ peaks at $\phi_c \sim 0.1$ and declines thereafter. At this volume fraction, D_{q^*} indicates an effective particle size of $D_c + 20$ nm. D_{q^*} is suggested to be a measure of the range over which the particle surface can influence polymer segment packing correlation, ~10 nm. This range is larger than the unperturbed molecular size of either polymer molecule, $12R_g$ and $8R_g$ in PEO400 and PEO1000, respectively. The Kuhn segment of PEO is calculated to be 1.2 nm; therefore, the repulsion is approximately eight segment diameters.

The particle structure factors imply that the particle surface is able to influence polymer properties far into the bulk polymer. Such behavior has been documented for polymer when confined between two plates and in dilute particle dispersion in polymer melts.[56−58] These studies suggest that confinement of polymer between two particles enhances the range over which the surface

can impact polymer properties. The sudden suppression in particle density fluctuations on increasing ϕ_c to a value larger than 0.1 is likely a confinement effect.

At a volume fraction of 0.2, the average interparticle separation distance, reaches 20 nm. At this volume fraction, $\phi_{S(q)}$ and D_{q^*} decline in a similar manner while $S(q,\phi_c)$ continues to resemble liquid like structure factors. The decline in $\phi_{S(q)}$ and D_{q^*} suggest that the range over which the particle can exert influence over the polymer is being reduced due to stripping of polymer from the interparticle region. This may explain the reduction in $\phi_{S(q)}$ and D_{q^*} while $S(q,\phi_c)$ continues to resemble liquid like structure factors.

In summary, we find that the particle pair interaction potential that drives how particles pack in the melt appears to not influence the viscosity. Classical statistical mechanics teaches us that the particle pair interaction potential should determine the particle density fluctuations as the particle phase becomes more concentrated, and this should in turn influence the particle dynamics and overall melt flow mechanics. The discrepancy between the rheology and the particle microstructure observed for these unentangled melts suggests that this view breaks down for filled melts studied here. Whereas the low shear viscosity collapses onto experimental hard spheres when the particle diameter is increased by $2.9R_g$, the static particle structure does not mimic this trend. The suppression of particle density fluctuations above and beyond those expected of hard particles suggests that internal configuration of the polymer and the ability of the polymer to associate with the particle play a role in determining microstructure. The results imply that the mixture of polymer and particles cannot be simply thought of as particles suspended in a solvent continuum even though $2R_g/D_c = 0.037$ for PEO400.

Acknowledgment. SBUSAXS data was collected at the X-ray Operations and Research beamline 32ID-B at the Advanced Photon Source (APS), Argonne National Laboratory. The APS is supported by the U.S. Department of Energy, Office of Science, Office of Basic Energy Sciences, under Contract No. DE-AC02-06CH11357. We appreciate our collaborative relationship and helpful discussions with Ken Schweizer. This work was supported by the Nanoscale Science and Engineering Initiative of the National Science Foundation under NSF Award Number DMR-0642573.

Note Added After ASAP Publication. This article was published ASAP on November 11, 2008. In Table 1, the viscosity of PEO400 has been changed. The correct version was published on December 2, 2008.

References and Notes

(1) Koo, J. H. *Polymer Nanocomposites*; McGraw-Hill: New York, 2006.
(2) Wang, M.-J. *Rubber Chem. Technol.* **1998**, *71*, 520.
(3) Lim, R.; Li, S. F. Y.; O'Shea, S. J. *Langmuir* **2002**, *18*, 6116–6124.
(4) Hooper, J. B.; Schweizer, K. S. *Macromolecules* **2005**, *38*, 8858–8869.
(5) Bitsanis, I.; Hadziioannou, G. *J. Chem. Phys.* **1990**, *92*, 3827–3847.
(6) Mansfield, K. F.; Theodorou, D. N. *Macromolecules* **1989**, *22*, 3143–3152.
(7) Granick, S.; Hu, H.-W. *Langmuir* **1994**, *10*, 3857–3866.
(8) Horn, R. G.; Hirz, S. J.; Hadziioannou, G.; Frank, C. W.; Catala, J. M. *J. Chem. Phys.* **1989**, *90*, 6767–6774.
(9) Horn, R. G.; Israelachvili, J. N. *Macromolecules* **1988**, *21*, 2836–2841.
(10) Hu, H.-W.; Granick, S. *Science* **1992**, *258*, 1339–1342.
(11) Israelachvili, J. N.; Kott, S. J. *J. Chem. Phys.* **1988**, *88*, 7162–7166.
(12) Luengo, G.; Schmitt, F. J.; Hill, R.; Israelachvili, J. *Macromolecules* **1997**, *30*, 2482–2494.
(13) Montfort, J. P.; Hadziioannou, G. *J. Chem. Phys.* **1988**, *88*, 7187–7196.
(14) Van Alsten, J.; Granick, S. *Macromolecules* **1990**, *23*, 4856–4862.
(15) Stark, R.; Bonaccurso, E.; Kappl, M.; Butt, H.-J. *Polymer* **2006**, *47*, 7259–7270.
(16) Sun, G.; Kappl, M.; Pakula, T.; Kremer, K.; Butt, H. J. *Langmuir* **2004**, *20*, 8030–8034.
(17) Degennes, P. G. *C. R. Acad. Sci. Ser. II* **1987**, *305*, 1181–1184.
(18) Israelachvili, J. N. *Intermolecular and surface forces*, 2nd ed.; Academic Press: New York, 1991.
(19) Le Meins, J. F.; Moldenaers, P.; Mewis, J. *Ind. Eng. Chem. Res.* **2002**, *41*, 6297–6304.
(20) Osman, M. A.; Atallah, A.; Schweizer, T.; Ottinger, H. C. *J. Rheol.* **2004**, *48*, 1167–1184.
(21) Sternstein, S. S.; Zhu, A. J. *Macromolecules* **2002**, *35*, 7262–7273.
(22) Zhang, Q.; Archer, L. A. *Langmuir* **2002**, *18*, 10435–10442.
(23) Zhu, Z. Y.; Thompson, T.; Wang, S. Q.; von Meerwall, E. D.; Halasa, A. *Macromolecules* **2005**, *38*, 8816–8824.
(24) Mackay, M. E.; Dao, T. T.; Tuteja, A.; Ho, D. L.; Van Horn, B.; Kim, H.; Hawker, C. J. *Nat. Mater.* **2003**, *2*, 762–766.
(25) Berriot, J.; Montes, H.; Martin, F.; Mauger, M.; Pyckhout-Hintzen, W.; Meier, G.; Frielinghaus, H. *Polymer* **2003**, *44*, 4909–4919.
(26) Aranguren, M. I.; Mora, E.; DeGroot, J. V.; Macosko, C. W. *J. Rheol.* **1992**, *36*, 1165–1182.
(27) Anderson, B. J.; Zukoski, C. F. *Macromolecules* **2007**, *40*, 5133–5140.
(28) Hooper, J. B.; Schweizer, K. S. *Macromolecules* **2006**, *39*, 5133–5142.
(29) Stöber, W.; Fink, A.; Bohn, E. *J. Colloid Interface Sci.* **1968**, *26*, 62–69.
(30) Kugler, J.; Fischer, E. W.; Peuscher, M.; Eisenbach, C. D. *Makromol. Chem.* **1983**, *184*, 2325–2334.
(31) Ho, D. L.; Hammouda, B.; Kline, S. R.; Chen, W. R. *J. Polym. Sci., Part B: Polym. Phys.* **2006**, *44*, 557–564.
(32) Balard, H.; Papirer, E.; Rahmani, Y.; Legrand, A. P.; Hommel, H. *Bull. Soc. Chim. Fr.* **1985**, 1139–1142.
(33) Hommel, H.; Legrand, A. P.; Balard, H.; Papirer, E. *Polymer* **1984**, *25*, 1297–1301.
(34) Russel, W. B.; Saville, D. A.; Schowalter, W. R. *Colloidal Dispersions*; Cambridge University Press: Cambridge, U.K., 1989.
(35) Anderson, B. J.; Gopalakrishnan, V.; Ramakrishnan, S.; Zukoski, C. F. *Phys. Rev. E (Stat., Nonlinear, Soft Matter Phys.)* **2006**, *73*, 031407.
(36) Ilavsky, J.; Allen, A. J.; Long, G. G.; Jemian, P. R. *Rev. Sci. Instrum.* **2002**, *73*, 1660–1662.
(37) George, A.; Wilson, W. W. *Acta Crystallogr., Sect. D: Biol. Crystallogr.* **1994**, *50*, 361–365.
(38) Kulkarni, A. M.; Chatterjee, A. P.; Schweizer, K. S.; Zukoski, C. F. *Phys. Rev. Lett.* **1999**, *83*, 4554–4557.
(39) Rosenbaum, D.; Zamora, P. C.; Zukoski, C. F. *Phys. Rev. Lett.* **1996**, *76*, 150–153.
(40) Rosenbaum, D. F.; Zukoski, C. F. *J. Cryst. Growth* **1996**, *169*, 752–758.
(41) Russel, W. B.; Saville, D. A.; Schowalter, W. R. *Colloidal Dispersions*; Cambridge University Press: Cambridge, U.K., 1992.
(42) Cichocki, B.; Felderhof, B. U. *J. Chem. Phys.* **1988**, *89*, 3705–3709.
(43) Cheng, Z.; Zhu, J.; Chaikin, P. M.; Phan, S.-E.; Russel, W. B. *Phys. Rev. E* **2002**, *65*, 041405.
(44) Phan, S.-E.; Russel, W. B.; Cheng, Z.; Zhu, J.; Chaikin, P. M.; Dunsmuir, J. H.; Ottewill, R. H. *Phys. Rev. E* **1996**, *54*, 6633.
(45) de Kruif, C. G.; van Iersel, E. M. F.; Vrij, A.; Russel, W. B. *J. Chem. Phys.* **1985**, *83*, 4717–4725.
(46) Mewis, J.; Frith, W. J.; Strivens, T. A.; Russel, W. B. *AIChE J.* **1989**, *35*, 415–422.
(47) Wyart, F. B.; de Gennes, P. G. *Eur. Phys. J. E: Soft Matter* **2000**, *1*, 93–97.
(48) Doi, M.; Edwards, S. F. *The theory of polymer dynamics*; Oxford University Press: New York, 1986.
(49) Schneider, H. M.; Frantz, P.; Granick, S. *Langmuir* **1996**, *12*, 994–996.
(50) Baxter, R. J. *J. Chem. Phys.* **1970**, *52*, 4559–4562.
(51) van Beurten, P.; Vrij, A. *J. Chem. Phys.* **1981**, *74*, 2744–2748.
(52) Vrij, A. *J. Chem. Phys.* **1979**, *71*, 3267–3270.
(53) Anderson, B. J.; Gopalakrishnan, V.; Ramakrishnan, S.; Zukoski, C. F. *Phys. Rev. E (Stat., Nonlinear, Soft Matter Phys.)* **2006**, *73*, 031407−031413.
(54) Payne, A. R. *J. Appl. Polym. Sci.* **1962**, *6*, 57–63.
(55) Granick, S.; Hu, H.-W.; Carson, G. A. *Langmuir* **1994**, *10*, 3867–3873.
(56) Van der Beek, G. P.; Stuart, M. A. C.; Fleer, G. J.; Hofman, J. E. *Macromolecules* **1991**, *24*, 6600–6611.
(57) Priestley, R. D.; Ellison, C. J.; Broadbelt, L. J.; Torkelson, J. M. *Science* **2005**, *309*, 456–459.
(58) Priestley, R. D.; Broadbelt, L. J.; Torkelson, J. M. *Macromolecules* **2005**, *38*, 654–657.
(59) McGuiggan, P. M.; Gee, M. L.; Yoshizawa, H.; Hirz, S. J.; Israelachvili, J. N. *Macromolecules* **2007**, *40*, 2126–2133.

MA801415E